Forward Stimulated Brillouin Scattering Analysis of Optical Fibers Coatings

Hilel Hagai Diamandi, Yosef London, Gil Bashan, Keren Shemer, and Avi Zadok

***Abstract*—The proper function of protective coating layers is essential for the handling and application of brittle optical fibers. The elastic parameters of polymer coatings can be studied through off-line analysis of test samples. However, the monitoring of these properties on a working fiber during service is challenging. In this work, we use forward stimulated Brillouin scattering processes in standard single mode fibers to measure the acoustic velocity in several types of coating layers. Pump light launches short acoustic pulses outward from the core of the fiber. Multiple reflections at the boundaries between cladding and coating, and between coating and air, form a series of delayed acoustic echoes across the core. These echoes are monitored, in turn, by photo-elastic phase modulation of probe light. Data are collected at temperatures between 25–120 °C. The thermal dependence of the acoustic velocities in several coatings and of the F-SBS resonance frequencies is investigated. Observations are corroborated by calculations. The proposed technique is well suited for research and development of coating materials, production line quality control, reliability studies and preventive maintenance of working fibers.**

***Index Terms*—Coatings, elastic constants, nonlinear fiber-optics, optical fiber sensors, opto-mechanics, stimulated brillouin scattering.**

I. Introduction

THE coating layers of brittle silica optical fibers are essential for their handling and deployment outside the research laboratory. In most applications, standard fibers are coated with thin polymer layers. Monitoring the elastic properties of these layers is important for research and development of new coating materials, production line quality control, reliability testing and preventive maintenance. In addition, elastic parameters of coating layers may be modified following adsorption of chemicals, and their assessment can serve towards sensing applications [1]. Elastic characterization protocols include dynamic strain-stress analysis [2], birefringence measurements [2], X-ray diffraction [3], surface acoustic wave microscopy [4], infrared spectrometry [5], glass transition monitoring [5], and more. However, all these techniques involve the off-line examination of test samples, and they are inapplicable to a working optical fiber. Methods for the in-service monitoring of elastic attributes of the coating layers are unavailable, to the best of our knowledge.

Forward stimulated Brillouin scattering (F-SBS) is a nonlinear optical effect that couples between two co-propagating optical fields and an acoustic wave that are guided in a common medium [6]–[18]. F-SBS has been studied in standard optical fibers since 1985 [6]. Unlike the more widely employed effect of backwards SBS, the acoustic modes that mediate forward Brillouin scattering in fibers are predominantly transverse [6]–[18]. These modes are guided by the whole fiber cross-section, and their transverse profiles span the entire cladding and reach its outer boundary [6]–[8]. The oscillations of the acoustic modes, and the entire F-SBS process, are therefore sensitive to the elastic properties of media beyond the fiber cladding. This characteristic serves as the basis for a new concept for optical fiber sensing of liquids outside the cladding boundary [19]–[26], which was first proposed by our group in 2016 [19].

The guided acoustic modes of optical fibers can reach into certain types of coating layers as well [27], [28]. Two separate recent studies, by the Thevenaz group at EPFL and by ourselves [27], [28], have formulated F-SBS processes in coated standard fibers. Both works demonstrated the quantitative analysis of liquids beyond the thin polyimide coating layer of commercially available fibers [27], [28]. However, these works considered the coating layer merely as an obstacle for the measurement of surrounding media.

In this work, we turn our attention to the F-SBS characterization of the coating layer itself. Pump light launches short acoustic pulses, outward from the core of the fiber, in the radial direction. Multiple reflections at the boundaries between cladding and coating, and between coating and air, form a series of delayed acoustic echoes across the core. These echoes are monitored, in turn, by photo-elastic phase modulation of a probe light. Data analysis retrieves the acoustic propagation delay across the coating layer. Several commercially-available coating types are examined. The results provide estimates of acoustic velocities and stiffness parameters in the coatings. The technique is perfectly suitable for working fibers and may be employed during service.

Measurements were performed at temperatures between 25–120 °C. The thermal sensitivity of the acoustic velocity in the coating layers is found to be 4–20 times larger than that of silica. In addition, the F-SBS resonance frequencies of individual guided acoustic modes were studied as functions of temperature. Analysis and measurements indicate that the frequencies of

Manuscript received September 13, 2020; revised November 1, 2020 and November 25, 2020; accepted November 25, 2020. Date of publication November 30, 2020; date of current version March 16, 2021. This work was supported in part by the Israel Ministry of Science and Technology under Grant 61047. *(Corresponding author: Avi Zadok.)*

The authors are with the Faculty of Engineering and Institute for Nano-Technology and Advanced Materials, Bar-Ilan University, Ramat-Gan 5290002, Israel (e-mail: hagaid@gmail.com; yoseflondon@gmail.com; gillbashan@gmail.com; shemerkeren@gmail.com; avinoam.zadok@biu.ac.il).

Color versions of one or more figures in this article are available at https://doi.org/10.1109/JLT.2020.3041352.

Digital Object Identifier 10.1109/JLT.2020.3041352

This work is licensed under a Creative Commons Attribution 4.0 License. For more information, see https://creativecommons.org/licenses/by/4.0/

specific modes change more strongly with temperature than those of others. High temperature sensitivity is closely linked with large modal confinement of acoustic energy in the coating layer. Agreement between experiments and calculations is very good.

The remainder of this paper is organized as follows: Section II provides a brief description of guided acoustic modes and F-SBS processes in coated standard fibers. The experimental setup and procedures are presented in Section III. Results of F-SBS characterization of fiber coatings and corresponding calculations are reported in Section IV. A concluding discussion is given in Section V.

II. Forward Stimulated Brillouin Scattering in Standard Coated Fibers

F-SBS in standard coated fibers has been analyzed and formulated in detail in [27], [28]. For the benefit of the reader, a brief description is given hereunder. Consider a standard single-mode silica fiber with a cladding radius a that is coated with a thin polymer layer of outer radius b. Throughout this work we assume that the coated fiber is kept in air (for the more general case of liquids with finite mechanical impedance outside the coating, see [27], [28]). The fiber supports the propagation of a discrete set of radial guided acoustic modes denoted by $R_{0,m}$, where m is an integer [6]–[8]. The transverse material displacement of these modes is in the radial direction only, and its transverse profile depends on the radial coordinate r only [6]–[8]. Each radial mode is characterized by a cut-off frequency Ω_m, below which it may not propagate [6]–[8]. When the temporal angular frequency of acoustic oscillations Ω is close to cut-off, the axial component of the acoustic wave-vector vanishes and the mode may be regarded as entirely transverse [6]–[8]. For most of this work we do not consider possible anisotropy in the coating material or geometric deviations from radial symmetry.

Let us denote the velocities of dilatational acoustic waves in the silica and coating layers as $V_{L1,2}$, respectively, and the corresponding radial wavenumbers as $p_{1,2} = \Omega/V_{L1,2}$. The radial modal profile of material displacement $U^{(m)}(r)$ [m] within the silica cladding $r \leq a$ is given by [29], [30]:

$$U_1^{(m)}(r) = p_1 \, A_3^{(m)} J_1(p_1 r). \tag{1}$$

The corresponding profile inside the coating $a \leq r \leq b$ equals [29], [30]:

$$U_2^{(m)}(r) = p_2 \left[A_1^{(m)} J_1(p_2 r) + A_2^{(m)} Y_1(p_2 r) \right]. \tag{2}$$

In Eq. (1) and Eq. (2), J_1 and Y_1 denote the first-order Bessel functions of the first and second kinds, respectively, and $A_{1,2,3}^{(m)}$ are constants (in units of m^2) whose values are determined by the boundary conditions (as explained later). The normal stresses in the radial direction in the two media may be expressed as [29], [30]:

$$T_{rr,1}^{(m)}(r) = c_{44,1} \, A_3^{(m)} \left[(p_1\kappa_1)^2 J_0(p_1 r) - \frac{2}{r} p_1 J_1(p_1 r) \right], \tag{3}$$

and

$$T_{rr,2}^{(m)}(r) = c_{44,2} (p_2\kappa_2)^2 \left[A_1^{(m)} J_0(p_2 r) + A_2^{(m)} Y_0(p_2 r) \right] - c_{44,2} \frac{2}{r} p_2 \left[A_1^{(m)} J_1(p_2 r) + A_2^{(m)} Y_1(p_2 r) \right]. \tag{4}$$

Here J_0 and Y_0 are the zero-order Bessel functions of the first and second kinds, respectively. The coefficients $c_{44,1}$ and $c_{44,2}$ are elements of the stiffness tensors $\boldsymbol{C}_{1,2}$ of silica and the coating material, respectively. Lastly, $\kappa_1^2 \equiv c_{11,1}/c_{44,1}$ and $\kappa_2^2 \equiv c_{11,2}/c_{44,2}$ denote stiffness ratios, where $c_{11,1}$ and $c_{11,2}$ are again elements of $\boldsymbol{C}_{1,2}$. The tensor elements are related to the acoustic velocities in the two media: $c_{11,i} = \rho_i \, V_{L,i}^2$ and $c_{44,i} = \rho_i \, V_{S,i}^2$, where $i = 1, 2$, ρ_i denote the denisities of silica and coating material respectively, and $V_{S,i}$ are the velocities of acoustic shear waves in the two media.

The boundary conditions of the elastic wave equation require the continuity of displacement and radial stress at the interface $r = a$ [29], [30]: $U_1^{(m)}(a) = U_2^{(m)}(a)$ and $T_{rr,1}^{(m)}(a) = T_{rr,2}^{(m)}(a)$, and zero stress at the outer boundary of the coating: $T_{rr,2}^{(m)}(b) = 0$. The three equations for $A_{1,2,3}^{(m)}$ have non-trivial solutions only for a discrete set of eigen-value frequencies Ω_m. Each eigen-value represents the cut-off frequency of a guided radial acoustic mode $R_{0,m}$ [28]. The corresponding eigen-vector solutions signify $A_{1,2,3}^{(m)}$ (except for a common complex magnitude that scales with the driving force). The cut-off frequencies therefore completely determine the transverse profiles of the acoustic modes. We express the displacement profiles as $U^{(m)}(r) = A^{(m)} \; u^{(m)}(r)$, with $u^{(m)}(r)$ [m^{-1}] normalized so that $(2\pi/\rho_1) \int_0^b \rho(r) |u^{(m)}(r)|^2 r dr = 1$. Here $\rho(r)$ denotes the local density. This form of normalization is more general than that of the bare fiber case, in which $\rho(r) = \rho_1$ [16].

The oscillations of the radial acoustic modes may be stimulated by a pump pulse of instantaneous power $P(t)$, where t stands for time, through the mechanism of electrostriction [6]–[8]. Let us denote the transverse profile of the single optical mode of the fiber as $E_T(r)$, normalized so that $2\pi \int_0^b |E_T(r)|^2 r dr = 1$, and the Fourier transform of $P(t)$ as $\tilde{P}(\Omega)$. The Frequency-domain magnitude of the stimulated modal displacement oscillations $\tilde{A}^{(m)}(\Omega)$ [$\mathrm{m}^2 \times \mathrm{rad}^{-1} \times \mathrm{Hz}^{-1}$] is given by [16], [28]:

$$\tilde{A}^{(m)}(\Omega) = \frac{Q_{ES}^{(m)}}{4nc\rho_1 \Omega_m \Gamma_m} \frac{1}{j - \Delta} \tilde{P}(\Omega). \tag{5}$$

Here n is the refractive index of silica, c denotes the speed of light in vacuum, and Γ_m is the modal linewidth which also represents the decay rate of acoustic intensity [16], [28]. With air outside the coating, the linewidth is solely determined by internal acoustic dissipation in the silica and coating material, and it is characterized experimentally. Also in Eq. (5), the normalized detuning parameter is defined as $\Delta \equiv 2(\Omega - \Omega_m)/\Gamma_m$, and $Q_{ES}^{(m)}$ expresses the modal overlap integral of electro-strictive

stimulation [16], [28]:

$$Q_{ES}^{(m)} = -\left(2a_1 + 4a_2\right) \cdot 2\pi \int_0^b \frac{\partial E_T\left(r\right)}{\partial r} E_T\left(r\right) u^{(m)}\left(r\right) r dr. \tag{6}$$

In Eq. (6), $a_{1,2}$ denote photo-elastic parameters of silica [16], [28]. When short pump pulses $P(t)$ are used, a packet of multiple radial acoustic modes is launched outward from the core of the fiber. The material displacement oscillations are associated with normal strain patterns in the fiber cross-section, in both the radial and the azimuthal directions [6]–[8]. Strain, in turn, induces photo-elastic perturbations to the local dielectric tensor, which oscillate at frequency Ω as well [6]–[8].

We consider next a weak, continuous optical probe field that is co-propagating in the fiber in the same direction as the pump pulse. The probe field is too weak to affect the stimulation of acoustic waves, nevertheless it is scattered by them. Due to photo-elasticity, the effective index seen by the probe light in every cross-section is oscillating at Ω with a magnitude $\Delta\tilde{n}^{(m)}(\Omega)$ [rad$^{-1}\times$Hz^{-1}] that is given by [16], [28]:

$$\Delta\tilde{n}^{(m)}\left(\Omega\right) \approx \frac{Q_{PE}^{(m)}}{2n} \tilde{A}^{(m)}\left(\Omega\right). \tag{7}$$

The modal overlap integral of photo-elastic perturbations is defined as [16], [28]:

$$Q_{PE}^{(m)} = \left(\frac{a_1 + a_2}{2}\right) 2\pi \int_0^b \left[\frac{\partial u^{(m)}\left(r\right)}{\partial r} + \frac{u^{(m)}\left(r\right)}{r}\right] \times \left|E_T\left(r\right)\right|^2 r dr. \tag{8}$$

Following propagation over a fiber of length L, the optical phase of the output probe wave is oscillating at Ω with a magnitude $\Delta\tilde{\varphi}^{(m)}\left(\Omega\right) = \Delta\tilde{n}^{(m)}\left(\Omega\right) k_0 L$, where k_0 is the vaccum wavenumber of the probe. Substituing Eqs. (5) and (7) yields:

$$\Delta\tilde{\varphi}^{(m)}\left(\Omega\right) = \frac{k_0 Q_{PE}^{(m)} Q_{ES}^{(m)}}{8n^2 c\rho_1 \Omega_m \Gamma_m} \frac{1}{j-\Delta} \tilde{P}\left(\Omega\right) L. \tag{9}$$

We may now define an equivalent modal nonlinear opto-mechanical coefficient $\gamma_{OM}^{(m)}(\Omega)$, in units of W$^{-1}\times$m^{-1}, so that $\Delta\tilde{\varphi}^{(m)}\left(\Omega\right) = \gamma_{OM}^{(m)}\left(\Omega\right)\tilde{P}(\Omega)L$ [16], [28]:

$$\gamma_{OM}^{(m)}\left(\Omega\right) = \frac{k_0 Q_{PE}^{(m)} Q_{ES}^{(m)}}{8n^2 c\rho_1 \Omega_m \Gamma_m} \frac{1}{j-\Delta} = \gamma_0^{(m)} \frac{1}{j-\Delta}. \tag{10}$$

The maximum magnitude of the opto-mechanical coefficient for each mode is reached on resonance:

$$\gamma_0^{(m)} = \frac{k_0 Q_{PE}^{(m)} Q_{ES}^{(m)}}{8n^2 c\rho_1 \Omega_m \Gamma_m}. \tag{11}$$

$|\gamma_{OM}^{(m)}(\Omega)|^2$ is also referred to as the F-SBS spectrum of the fiber. The instantaneous phase modulation of the probe wave at the fiber output due to F-SBS, $\Delta\varphi(t)$, is given by the inverse Fourier transform of $\sum_m \Delta\tilde{\varphi}^{(m)}(\Omega)$. For short pump pulses, $\Delta\varphi(t)$ consists of multiple reflected echoes from the boundaries between cladding and coating and between coating and air. The instantaneous phase modulation and spectrum of F-SBS are affected, among other parameters, by the elastic properties of the coating layer.

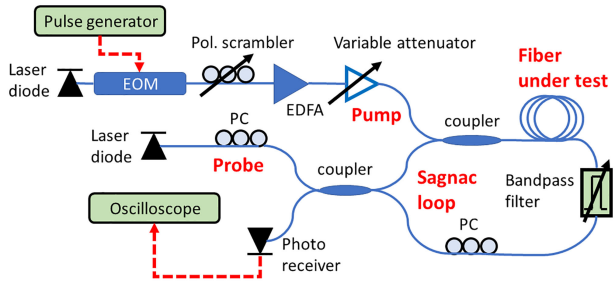

Fig. 1. Schematic illustration of the experimental setup for forward stimulated Brillion scattering measurements. EOM: electro-optic amplitude modulator; EDFA: erbium-doped fiber amplifier; PC: polarization controller.

III. Experimental Setup and Procedures

F-SBS processes were characterized using pump-probe experiments as shown in Fig. 1 [12], [19], [28]. Light from a first laser diode at 1550 nm wavelength was modulated into short and isolated pump pulses of 1.2 ns duration and 5 μs period using an electro-optic amplitude modulator. The broadband pulses excite a packet of multiple acoustic modes. In several previous studies (see for example Fig. 3 of [12]), continuous pump waves were modulated at specific radio frequencies to stimulate individual acoustic modes. F-SBS process in fibers may be effectively characterized using both protocols.

The pump pulses were amplified by an erbium-doped fiber amplifier and launched into a section of fiber under test that was embedded in a Sagnac interferometer loop ([12], see Fig. 1). Pump pulses were coupled into the fiber in the clockwise direction only, and were blocked from reaching the loop output by a tunable optical bandpass filter (BPF). The average power of pump pulses was changed between 60–300 mW using a variable optical attenuator. Stronger pump pulses were used for shorter fiber samples, and vice versa. The power levels were adjusted to obtain comparable F-SBS magnitudes across all test samples.

The pump pulses stimulated the oscillations of radial guided acoustic modes of the fiber under test as described in the previous section. A polarization scrambler was used to eliminate the potential contributions of more general, torsional-radial guided acoustic modes to the F-SBS process measurements [12], [19], [28]. The temporal shape of the pump pulses $P(t)$ was recorded, and its Fourier transform $\tilde{P}(\Omega)$ was calculated offline and used in data analysis (see below).

A continuous probe wave from a second laser diode source at 1532 nm wavelength was coupled into the loop in both directions. The BPF inside the loop was aligned to transmit the probe wavelength. F-SBS induced phase modulation $\Delta\varphi(t)$ to the clockwise-propagating probe wave, as discussed above. For the fibers lengths and the pump power levels used in this work, $\Delta\varphi(t) \ll 2\pi$. Due to the forward scatter characteristics of the process, the counter-clockwise propagating probe wave was largely unaffected [6]–[8], [12], [19], [28]. The non-reciprocal phase modulation due to F-SBS is converted to intensity modulation of the probe wave at the Sagnac loop output. The output probe wave was detected by a photo-receiver of responsivity $R = 27$ [V$\times$W^{-1}]. Polarization controllers (PCs) were used to

TABLE I
FIBERS UNDER TEST

Sample	Coating	Diameter [μm]	Length [m]
Reference	Bare fiber	$2a = 125 \pm 0.5$	$L = 6$
A	Polyimide 1	$2b = 148 \pm 0.5$	$L = 10$
B	Polyimide 2	$2b = 141 \pm 0.5$	$L = 100$
C	Polyimide 2	$2b = 155 \pm 0.5$	$L = 100$
D	Fluoroacrylate	$2b = 136 \pm 0.5$	$L = 7$

TABLE II
ELASTIC PARAMETERS USED IN F-SBS CALCULATIONS

Material (sample)	Density [kg×m^{-3}]	Stiffness ratio
Silica (all)	$\rho_1 = 2200$ [32]	$\kappa_1 = 1.586$ [32]
Polyimide 1 (A)	$\rho_2 = 1420$ [28]	$\kappa_2 = 2.031$[28]
Polyimide 2 (B,C)	$\rho_2 = 1420$ [28]	$\kappa_2 = 2.031$ [28]
Fluoroacrylate (D)	$\rho_2 = 1200$ [28]	$\kappa_2 = 2.031$[28]

adjust the bias value of non-reciprocal phase delay between the two directions of propagation of the probe wave [19], [28]. Given proper bias adjustments [19], [28], the detected voltage $V(t)$ is simply related to the F-SBS phase modulation:

$$V(t) \approx RP_s \left[1 + \Delta\varphi(t)\right]. \tag{12}$$

Here $P_s = 2$ mW is the probe power at the loop output with the pump pulses turned off. The detector output voltage was sampled using a real-time digitizing oscilloscope for further offline processing.

In addition to F-SBS, the probe wave also undergoes cross-phase modulation by the pump pulses via the Kerr effect. However, the contribution of the instantaneous Kerr effect vanishes as soon as the pump pulse ends, whereas phase modulation through F-SBS continues for hundreds of nanoseconds or longer. Time gating of collected $V(t)$ traces removes the Kerr effect from the analysis of probe phase modulation [19], [28]. The normalized F-SBS spectrum of the fiber under test is estimated using the radio-frequency power spectrum $|\tilde{V}(\Omega)|^2$ of the gated traces:

$$\left|\gamma_{OM}^{(m)}(\Omega)\right|^2 \propto \left|\tilde{V}(\Omega)\right|^2 / \left|\tilde{P}(\Omega)\right|^2. \tag{13}$$

Data were collected for several samples of standard, single-mode silica fibers with 125 μm cladding diameter and different types of coating. The outer diameters of the fibers were measured using a precision micrometer. The coating parameters are summarized in Table I. In several experiments the fiber under test was placed in a variable-temperature chamber. Measurements results are reported in the next section.

IV. RESULTS

Fig. 2(a) shows the measured output voltage $V(t)$ for a reference bare fiber sample at room temperature. The F-SBS phase modulation of the probe wave consists of a series of impulses, separated by an acoustic propagation delay of 20.8 $\pm$ 0.1 ns. The events correspond to successive reflections of a stimulated acoustic wave-packet at the outer boundary of the exposed cladding. The time difference between events corresponds to an acoustic velocity $V_{L,1}$ of 6,010 $\pm$ 50 m×s^{-1}, in agreement with the known value for silica [31]. The experimental error is dominated by uncertainty in the cladding diameter. The normalized F-SBS spectrum of the bare fiber is shown in Fig. 2(b). The spectrum consists of a series of sparse and narrow resonances, which correspond to the stimulation of $R_{0,m}$ modes. The frequencies and the relative magntiudes of the spectral peaks agree with previous observations [6], [10], [19].

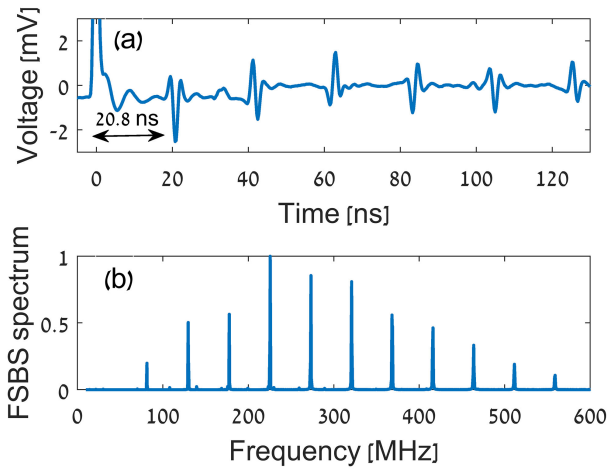

Fig. 2. (a) Instantaneous output voltage of the detected probe wave following F-SBS phase modulation in a reference, bare fiber sample. The acoustic propagation delay of 20.8 ns between successive reflection events is noted. (b) Measured normalized F-SBS spectrum of a reference, bare fiber sample.

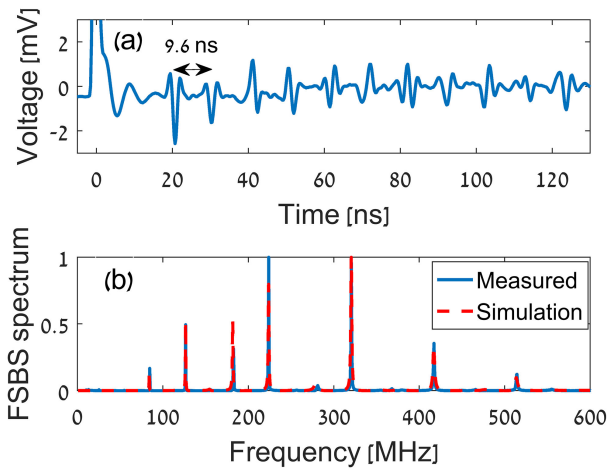

Fig. 3. (a) Instantaneous output voltage of the detected probe wave following F-SBS phase modulation in fiber sample A. The two-way acoustic propagation delay across the coating of 9.6 ns is noted. (b) Measured (solid blue) and calculated (dashed red) normalized F-SBS spectra of fiber sample A.

Fig. 3(a) presents the temporal trace of the output voltage obtained for fiber sample A (see Table I), at room temperature. A first impulse is observed 20.8 ns following the pump pulse. This first event corresponds to a partial reflection of the acoustic wave-packet at the interface between the silica fiber cladding and the polyimide coating layer. A second impulse occurs 9.6 $\pm$ 0.1 ns after the first one. This second event is due to an

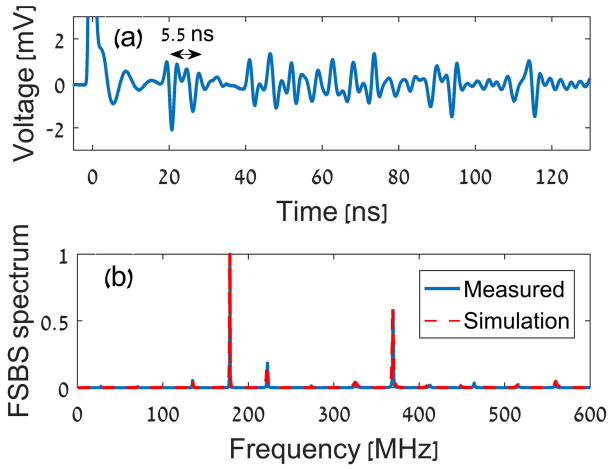

Fig. 4. (a) Instantaneous output voltage of the detected probe wave following F-SBS phase modulation in fiber sample B. The two-way acoustic propagation delay across the coating of 5.5 ns is noted. (b) Measured (solid blue) and calculated (dashed red) normalized F-SBS spectra of fiber sample B.

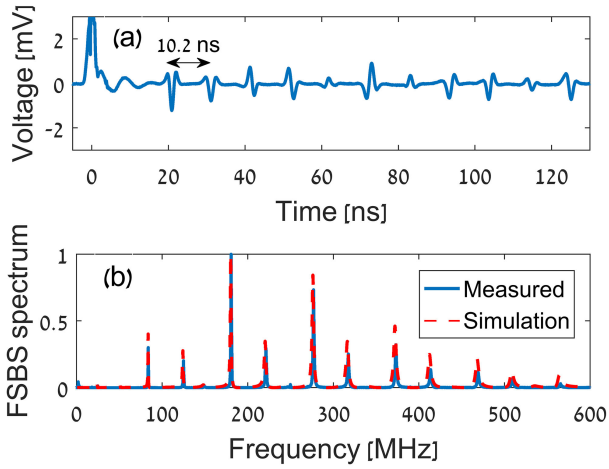

Fig. 5. (a) Instantaneous output voltage of the detected probe wave following F-SBS phase modulation in fiber sample C. The two-way acoustic propagation delay across the coating of 10.2 ns is noted. (b) Measured (solid blue) and calculated (dashed red) normalized F-SBS spectra of fiber sample C.

acoustic reflection at the outer boundary of the coating. The time difference between the two impulses represents the two-way propagation delay of a dilatational acoustic wave-packet across the coating layer. The acoustic velocity $V_{L,2}$ in the coating of fiber A at room temperature is estimated as 2380 ± 50 m×s^{-1}.

Fig. 3(b) shows the measured and calculated normalized F-SBS spectra of fiber sample A. The linewidths Γ_m used in calculations were taken from the measurements. The linewidths for polyimide coating are in agreement with previous work [28]. The value of $c_{44,2} = 1.95$ GPa was fitted based on the above measured velocity $V_{L,2}$ and on literature values of ρ_2 and κ_2 (see Table II). The elastic parameters were assumed to be independent of frequency. The agreement between experiment and model is very good.

We carried out numerical calculations of the acoustic modes of fiber sample A with an elliptical or non-concentric coating layer, using a commercial solver platform. The results indicate that ellipticity or non-concentricity by up to 1 micron have little effect on the F-SBS spectrum, and the modal cut-off frequencies shift by less than 1%. Larger geometric variations may considerably change the transverse profiles of the radial acoustic modes, affect their spatial overlap with guided light and qualitatively modify the forward SBS spectrum. The good agreement between measurements and the radially symmetric coating model suggests that deviations from radial symmetry in the coating of the fiber sample were likely below 1 micron.

Fig.s 4 through 6 show the measured $V(t)$ traces and the experimental and calculated F-SBS spectra of test samples B, C and D, respectively. The acoustic velocities in the three samples are estimated as 2900 ± 80, 2940 ± 60 and 1870 ± 80 m×s^{-1}. Note that samples B and C are coated with the same polyimide material, with different outer diameters. The measured velocities $V_{L,2}$ for the two samples differ by less than 1.5%. The signal-to-noise ratio in the measurement of sample D is lower than those of the other fibers, due to larger acoustic dissipation in the fluoroacrylate polymer. Agreement between model and measurement is less complete for fiber D. A possible explanation is anisotropy or lack of symmetry in the coating layer.

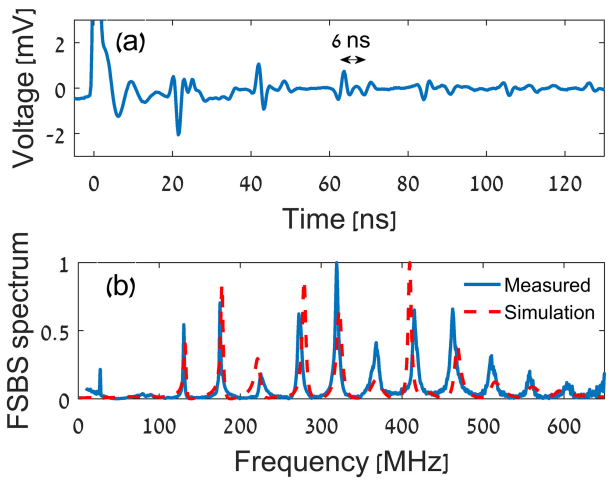

Fig. 6. (a) Instantaneous output voltage of the detected probe wave following F-SBS phase modulation in fiber sample D. The two-way acoustic propagation delay across the coating of 6.0 ns is noted. (b) Measured (solid blue) and calculated (dashed red) normalized F-SBS spectra of fiber sample D.

Fig. 7 shows the measured acoustic velocities $V_{L,2}$ in the coatings of samples A, B and D as functions of temperature T, between 25–120 °C. The exact temperature during each acquisition was calibrated through the F-SBS process itself, using measurements of the acoustic propagation delay across the silica cladding. The acoustic velocity $V_{L,1}$ in silica is known to vary by 0.6 m×s^{-1} per °K [31]. The acoustic velocities in the coatings decrease with temperature, with slopes of -2.4, -2.2 and -12.2 m×s^{-1} per °K for samples A, B and D, respectively. The results suggest that the coating stiffness parameter $c_{11,2}$ is reduced by 15% for fiber A, and by as much as 74% for fiber D, between 25–100 °C. Thermal changes in density are assumed to be much smaller [2], [3].

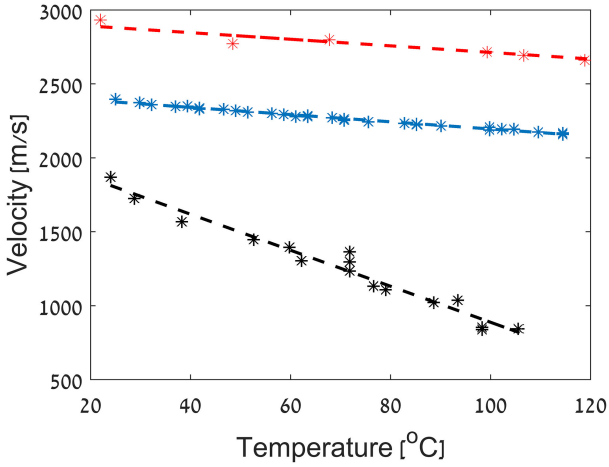

Fig. 7. Measured velocities of dilatational acoustic waves in the coating layers of fiber samples A (blue), B (red) and D (black). Markers denote experimental data, dashed lines represent linear fits.

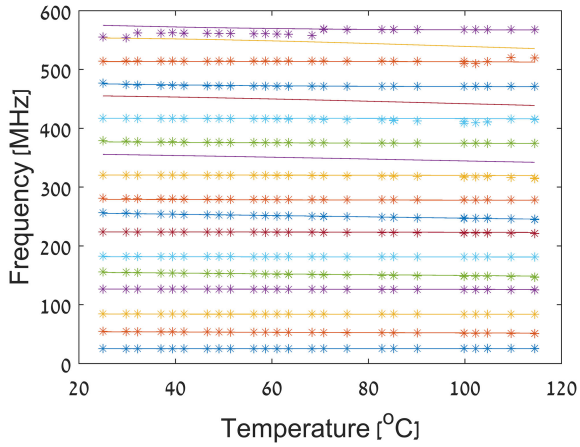

Fig. 9. Measured (asterisk markers) and calculated (solid lines) resonance frequencies of F-SBS in fiber sample A, as functions of temperature. Colors denote different radial modes, from $R_{0,1}$ (lowest frequency) to $R_{0,18}$ (highest frequency).

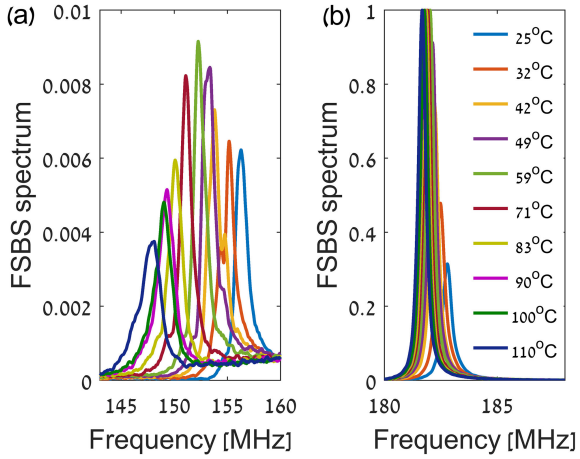

Fig. 8. Magnified views of measured normalized F-SBS spectra of fiber sample A at several temperatures (see legend in panel (b)). (a) Mode $R_{0,5}$. (b) Mode $R_{0,6}$.

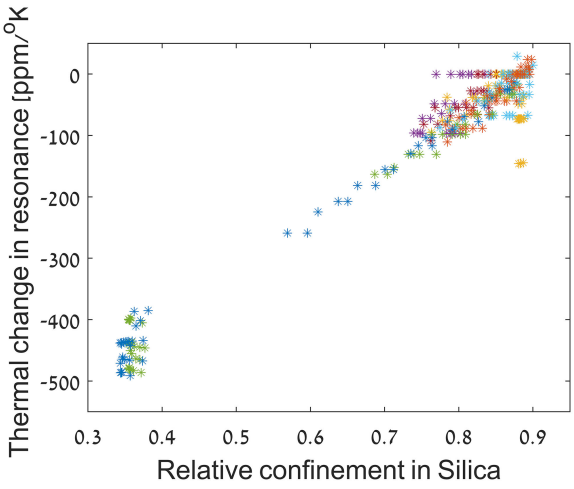

Fig. 10. Thermal sensitivity of the F-SBS resonance frequency (vertical axis) against the relative modal confinement of acoustic energy in the silica cladding (horizontal axis), for fiber sample A. Data were accumulated over all temperatures tested, and all experimentally observed radial modes. Colors follow those of Fig. 9. The two metrics are closely correlated.

The changes of the F-SBS resonance frequencies with temperature were examined as well. Fig. 8 shows magnified views of parts of the F-SBS spectra of fiber sample A at several temperatures. The resonance frequency of mode $R_{0,6}$ near 182 MHz is comparatively stable over the range of temperatures tested, and remains within a limit of only ± 0.6 MHz. By contrast, the frequency of mode $R_{0,5}$ near 150 MHz changes by as much as ± 4.2 MHz across the same temperature range. Fig. 9 shows the measured and calculated resonance frequencies of all F-SBS peaks of fiber A up to 600 MHz, as functions of temperature. The stiffness parameters used in the simulation were modified for each temperature based on the measured $V_{L,2}(T)$. Thermal variations of densities $\rho_{1,2}$, radii a and b or ratios $\kappa_{1,2}$ were neglected with respect to much larger changes in stiffness [2], [3]. Close agreement between measured and calculated frequencies is observed across the entire temperature range.

Similar to the examples of Fig. 8, the resonance frequencies of certain modes vary more strongly with temperature than those of others. In a few cases the calculated cut-off frequencies of adjacent modes draw near each other (see for example modes $R_{0,17}$ and $R_{0,18}$, the highest orders shown in the figure). The F-SBS spectra of the two modes partially overlap, and the experiments show a peak in between the two predicted modal cut-off frequencies. Radial acoustic modes $R_{0,11}$ and $R_{0,14}$ were not observed in the measured F-SBS spectra, due to poor spatial overlap with the optical mode.

Insight into the differences in temperature dependence among modes may be gained through the analysis of modal confinement. Thermal variations of stiffness in the coating of fiber A are larger than in silica. We therefore anticipate that acoustic modes which are more strongly confined to the coating would exhibit greater sensitivity to temperature. Fig. 10 plots the calculated normalized thermal sensitivity of the F-SBS resonance frequencies in sample A: $\alpha_T \equiv [\partial \Omega_m / \partial T]/\Omega_m$, against the

calculated fraction of acoustic energy in the silica cladding: $\delta \equiv (2\pi/\rho_1)\int_0^a \rho(r)|u^{(m)}(r)|^2 r dr$. Data were accumulated over all modes that were observed experimentally and all temperatures tested. The two metrics are closely correlated, as expected: Modes that are largely confined in the silica cladding exhibit comparatively smaller values of α_T, whereas those with higher confinement in the coating layer are characterized by stronger thermal sensitivity of their resonance frequencies.

V. Discussion

In this work, we have proposed and demonstrated the measurement of acoustic velocity in the coating layer of standard working fibers using F-SBS processes. An optical pump wave stimulates short acoustic pulses that propagate outward in the radial direction, from the core of the fiber towards its outer boundary. Multiple acoustic reflections take place at the two interfaces: between cladding and coating and between coating and air. These reflections form delayed acoustic pulse echoes in the fiber core. The echoes, in turn, are monitored through the photo-elastic phase modulation of probe light. The F-SBS process therefore provides an elastic echogram of the fiber cross-section. Acoustic transduction and detection are carried out using light alone. The timing of reflected echoes retrieves the acoustic velocity in the coating layer, and provides an estimate of the stiffness parameters in the layer.

Measurements were performed across a temperature range between 25–120 °C. The acoustic velocities in the coating layers decrease with temperature by -2.2 to -12.2 $\mathrm{m}\times\mathrm{s}^{-1}$ per °K. The temperature variations are 4–20 times larger than that of the acoustic velocity in the silica cladding, and they are of the opposite sign. The results also reveal the temperature dependence of specific modal resonance frequencies, which is consistent with the relative modal confinement of acoustic energy in the coating layer. The different sensitivities to temperature changes across numerous modes may help disambiguate multi-parameter analysis. Note that the measurement protocol also includes inherent temperature monitoring based on the acoustic time of flight through the silica cladding.

The proposed method is perfectly suitable for studying the coating layers of working fibers: in research and development, production line quality control, reliability testing and in-service maintenance. The measurement of acoustic velocity identifies changes in the stiffness of the coating layer, on the level of a few percent. Variations in stiffness, either with time or across fiber segments, provide early indication of failure or insufficient process control. The proposed method may also identify deviations from radial symmetry of the coating layer. In-service monitoring could be particularly useful in fiber sensors, which are often installed in aggressive environments and/or critical infrastructure. The proposed testing method can identify early signs of fatigue in the sensing fiber and enable preventive maintenance. In-service monitoring can also extend the service life of installed fibers, as safety margins for their replacement timeline may be reduced.

The measurement technique is also suitable for chemical or biological sensors of surrounding media, based on the effects of adsorbed reagents or environmental conditions on the elastic properties of the coating [1]. Such effects might be observed even when the condition of interest has no direct implication on the optical properties of the fiber, or could complement measurements of optical metrics. F-SBS characterization of coating layers can be extended to spatially-distributed analysis using several recently established protocols [23]–[26], [28]. The state-of-the-art spatial resolution of forward SBS analysis is several meters [25], [26]. Modifications to the coating would have to reach a comparable extent for proper detection. However, the resolution of forward SBS analysis protocols advances rapidly, with an order of magnitude improvement this year alone [25], [26].

F-SBS analysis is not applicable to all coating layers: For example, the standard acrylate coating absorbs the acoustic waves that are launched from within the fiber, and keeps them from reaching its outer boundary. Nevertheless, the results show that the method is applicable to several coatings. These include polyimide layers that are designed for harsh environments, where reliability and careful monitoring are of particular significance. The modelling in this work has been restricted for the most part to isotropic coatings that are radially symmetric. The numerical analysis of F-SBS in fibers with an anisotropic or with a non radially symmetric coating may be extended further. A comprehensive study is outside the scope of the present work. Deviations from symmetry may considerably modify the F-SBS spectra and increase the uncertainty in the estimates of acoustic velocity.

In conclusion, F-SBS opens up the elastic analysis of coatings outside working fibers, which is yet to be reported, with large potential implications in the optical fibers industry. Future work would employ F-SBS analysis to additional coating types and over a broader range of temperatures, and explore sensing applications.

Acknowledgment

Hilel Hagai Diamandi is grateful to the Azrieli Foundation for the award of an Azrieli Fellowship. Gil Bashan is supported by the Adams Fellowship Program of the Israel Academy of Sciences and Humanities.

References

[1] P. Kronenberg, P. K. Rastogi, P. Giaccari, and H. G. Limberger, "Relative humidity sensor with optical fiber Bragg gratings," *Opt. Lett.*, vol. 27, no. 16, pp. 1385–1387, Aug. 2002.

[2] J. C. Coburn, M. T. Pottiger, S. C. Noe, and S. D. Senturia, "Stress in polyimide coatings," *J. Polym. Sci., Part B: Polym. Phys.*, vol. 32, no. 7, pp. 1271–1283, May 1994.

[3] S. I. Numata, S. Oohara, K. Fujisaki, J. I. Imaizumi, and N. Kinjo, "Thermal expansion behavior of various aromatic polyimides," *J. Appl. Polym. Sci.*, vol. 31, no. 1, pp. 101–110, Jan. 1986.

[4] R. Logan, A. A. Maznev, K. A. Nelson, and J. Megusar, "Photothermal/photoacoustic method for in situ evaluation of radiation-hardened polyimide films," *J. Nucl. Mater.*, vol. 246, no. 2-3, pp. 256–259, Aug. 1997.

[5] J. Megusar, "Low temperature fast-neutron and gamma irradiation of kapton polyimide films," *J. Nucl. Mater.*, vol. 245, no. 2–3, pp. 185–190, Jun. 1997.

[6] R. M. Shelby, M. D. Levenson, and P. W. Bayer, "Guided acoustic-wave brillouin scattering," *Phys. Rev. B*, vol. 31, no. 8, pp. 5244–5252, Apr. 1985.
[7] A. S. Biryukov, M. E. Sukharev, and E. M. Dianov, "Excitation of sound waves upon propagation of laser pulses in optical fibers," *J. Quant. Elect.*, vol. 32, no. 9, pp. 765–775, Sep. 2002.
[8] P. St. J. Russell, D. Culverhouse, and F. Farahi, "Experimental observation of forward stimulated brillouin scattering in dual-mode single-core fibre," *Elect. Lett.*, vol. 26, no. 15, pp. 1195–1196, Jul. 1990.
[9] E. Peral and A. Yariv, "Degradation of modulation and noise characteristics of semiconductor lasers after propagation in optical fiber due to a phase shift induced by stimulated brillouin scattering," *IEEE J. Quant. Elect.*, vol. 35, no. 8, pp. 1185–1195, Aug. 1999.
[10] J. Wang, Y. Zhu, R. Zhang, and D. J. Gauthier, "FSBS resonances observed in standard highly nonlinear fiber," *Opt. Express*, vol. 19, no. 6, pp. 5339–5349, Mar. 2011.
[11] P. Dainese *et al.*, "Stimulated brillouin scattering from multi-GHz-guided acoustic phonons in nanostructured photonic crystal fibres," *Nat. Phys.*, vol. 2, no. 6, pp. 388–392, Jun. 2006.
[12] M. S. Kang, A. Nazarkin, A. Brenn, and P. St. J. Russell, "Tightly trapped acoustic phonons in photonic crystal fibers as highly nonlinear artificial raman oscillators," *Nat. Phys.*, vol. 5, no. 3, pp. 276–280, Mar. 2009.
[13] M. Pang, W. He, X. Jiang, and P. St. J. Russell, "All-optical bit storage in a fibre-laser by optomechanically bound states of solitons," *Nat. Photon.*, vol. 10, no. 5, pp. 454–458, May 2016.
[14] R. Van Laer, B. Kuyken, D. van Thourhout, and R. Baets, "Interaction between light and highly confined hypersound in a silicon photonic nanowire," *Nat. Photon.*, vol. 9, no. 3, pp. 199–203, Mar. 2015.
[15] E. A. Kittlaus, H. Shin, and P. T. Rakich, "Large brillouin amplification in silicon," *Nat. Photon.*, vol. 10, no. 6, pp. 463–467, Jun. 2016.
[16] H. H. Diamandi, Y. London, and A. Zadok, "Opto-mechanical inter-core cross-talk in multi-core fibers," *Optica*, vol. 4, no. 3, pp. 289–297, Mar. 2017.
[17] H. H. Diamandi, Y. London, G. Bashan, A. Bergman, and A. Zadok, "Highly-coherent stimulated phonon oscillations in a multi-core optical fibers," *Sci. Rep.*, vol. 8, Jun. 2018. Art. no. 9514.
[18] H. H. Diamandi *et al.*, "Opto-mechanical interactions in multi-core optical fibers and their applications," *J. Sel. Top. Quantum Electron.*, vol. 26, no. 4, pp. 1–13, Jul./Aug. 2020. Art. no. 2600113.
[19] Y. Antman, A. Clain, Y. London, and A. Zadok, "Optomechanical sensing of liquids outside standard fibers using forward stimulated brillouin scattering," *Optica*, vol. 3, no. 5, pp. 510–516, May 2016.
[20] N. Hayashi, Y. Mizuno, K. Nakamura, S. Y. Set, and S. Yamashita, "Experimental study on depolarized GAWBS spectrum for optomechanical sensing of liquids outside standard fibers," *Opt. Express*, vol. 25, no. 3, pp. 2239–2244, Feb. 2017.
[21] D. Chow, M. A. Soto, and L. Thévenaz, "Frequency-domain technique to measure the inertial response of forward stimulated brillouin scattering for acoustic impedance sensing," in *Proc. 25th Int. Opt. Fiber Sensors Conf.*, Apr. 2017, pp. 1–4.
[22] N. Hayashi, Y. Mizuno, K. Nakamura, S. Y. Set, and S. Yamashita, "Characterization of depolarized GAWBS for optomechanical sensing of liquids outside standard fibers," in *Proc. 25th Opt. Fibre Sensors Conf.*, Apr. 2017, pp. 1–4.
[23] G. Bashan, H. H. Diamandi, Y. London, E. Preter, and A. Zadok, "Optomechanical time-domain reflectometry," *Nat. Commun.*, vol. 9, Jul. 2018. Art. no. 2991.
[24] D. Chow, Z. Yang, M. A. Soto, and L. Thévenaz, "Distributed forward brillouin sensor based on local light phase recovery," *Nat. Commun.*, vol. 9, Jul. 2018. Art. no. 2990.
[25] S. Zaslawski, Z. Yang, S. Wang, and L. Thévenaz, "Distributed forward stimulated brillouin scattering measurement using broadband BOTDR," in *Proc. 7th Eur. Workshop Opt. Fibre Sensors*, vol. 11199, Aug. 2019, Art. no. 1119923.
[26] C. Pang *et al.*, "Opto-mechanical time-domain analysis based on coherent forward stimulated brillouin scattering probing," *Optica*, vol. 7, no. 2, pp. 176–184, Feb. 2020.
[27] D. M. Chow and L. Thévenaz, "Forward brillouin scattering acoustic impedance sensor using thin polyimide-coated fiber," *Opt. Lett.*, vol. 43, no. 21, pp. 5467–5470, Nov. 2018.
[28] H. H. Diamandi, Y. London, G. Bashan, and A. Zadok, "Distributed opto-mechanical analysis of liquids outside standard fibers coated with polyimide," *Appl. Phys. Lett. – Photon.*, vol. 4, no. 1, Jan. 2019. Art. no. 016105.
[29] P. B. Nagy, "Longitudinal guided wave propagation in a transversely isotropic rod immersed in fluid," *J. Acoust. Soc. Amer.*, vol. 98, no. 1, pp. 454–457, Jul. 1995.
[30] A. H. Nayfeh and P. B. Nagy, "General study of axisymmetric waves in layered anisotropic fibers and their composites," *J. Acoust. Soc. Amer.*, vol. 99, no. 2, pp. 931–994, Feb. 1996.
[31] H. J. McSkimin, "Measurement of ultrasonic wave velocities and elastic moduli for small solid specimens at high temperatures," *J. Acoust. Soc. Amer.*, vol. 31, no. 3, pp. 287–295, Mar. 1959.
[32] H. E. Engan, B. Y. Kim, J. N. Blake, and H. J. Shaw, "Propagation and optical interaction of guided acoustic waves in two-mode optical fibers," *J. Lightw. Technol.*, vol. 6, no. 3, pp. 428–436, Mar. 1988.

Hilel Hagai Diamandi received the B.Sc. and M.Sc. degrees in electrical engineering from Bar-Ilan University, Israel, in 2015 and 2017, respectively. He is currently working toward the Ph.D. degree in electrical engineering with Bar-Ilan University. His research interests include optical fiber sensors and opto-mechanical interactions in optical fibers. Mr. Diamandi was the recipient of the Bar-Ilan University Rector Award for excellence in undergraduate studies twice: in 2013 and 2015, and the same Award for excellence in graduate studies in 2017. In 2018, he was awarded the Azrieli Fellowship for doctoral studies by the Azrieli Foundation.

Yosef London received the B.Sc. degree in physics and electrical engineering in 2013, the M.Sc. degree in electrical engineering in 2015, and the Ph.D. degree in electrical engineering in 2020, all from Bar-Ilan University, Israel. He is currently a Postdoctoral Fellow with Soreq National Research Center in Yavne, Israel. His research interests include optical fiber sensors, nonlinear optics, and opto-mechanical interactions in fibers and photonic integrated circuits. Dr. London was the recipient of the Bar-Ilan University Rector Award for excellence in graduate studies in 2015.

Gil Bashan received the B.Sc. degree in physics and electrical engineering and the M.Sc. degree in electrical engineering from Bar-Ilan University, Israel, in 2016 and 2018, respectively. He is currently working toward the Ph.D. degree in electrical engineering. His research interests include optical fiber propagation effects, opto-mechanics, and Brillouin scattering. Mr. Bashan was the recipient of the Bar-Ilan University Rector Award for excellence in graduate studies in 2018. In 2020 he was awarded the Adams Fellowship for doctoral studies by the Israel National Academy of Sciences and Humanities.

Keren Shemer received the B.Sc. degree in physics and electrical engineering and the M.Sc. degree in electrical engineering from Tel-Aviv University, Israel in 2009 and 2015 (cum laude), respectively. She is currently working toward the Ph.D. degree in electrical engineering with Bar-Ilan University, Israel. Her research interests include fiber-optic sensors, fiber opto-mechanics, and laser range-finder protocols.

Avi Zadok received the B.Sc. degree in physics and mathematics from the Hebrew University of Jerusalem, Israel in 1994, the M.Sc. degree in physical electronics from Tel-Aviv University, Israel in 1999, and the Ph.D. degree in electrical engineering from Tel-Aviv University in 2007. Between 2007 and 2009, he was a Postdoctoral Research Fellow at the Department of Applied Physics, California Institute of Technology Pasadena, USA. In 2009, he joined the Faculty of Engineering, Bar-Ilan University, Israel, where he has been a Full Professor since 2017. He is the co-author of 150 papers in scientific journals and proceedings of international conferences. His research interests include fiber-optics, nonlinear optics, integrated photonic devices, and opto-mechanics. Dr. Zadok was the recipient of the Krill Award of the Wolf Foundation in 2013. He received a Starter Grant from the European Research Council (ERC) in 2015. Dr. Zadok was a member of the Israel Young Academy (2016–2020), and was its Chairman from 2019 to 2020.